International Journal of Modern Physics B, Vol. 16, No. 4 (2002) 531–561

OPTIMIZING THE SPEED OF A JOSEPHSON JUNCTION WITH DYNAMICAL MEAN FIELD THEORY

J. K. FREERICKS
Department of Physics, Georgetown University, Washington, DC 20057, USA

B. K. NIKOLIĆ
Department of Physics, Georgetown University, Washington, DC 20057, USA

P. MILLER
Department of Physics, Brandeis University, Waltham, MA 02454, USA

Received 25 September 2001

We review the application of dynamical mean-field theory to Josephson junctions and study how to maximize the characteristic voltage I_cR_n which determines the width of a rapid single flux quantum pulse, and thereby the operating speed in digital electronics. We study a wide class of junctions ranging from SNS, SCmS (where Cm stands for correlated metal), SINIS (where the insulating layer is formed from a screened dipole layer), and SNSNS structures. Our review is focused on a survey of the physical results; the formalism has been developed elsewhere.

1. Introduction

The DC Josephson effect,[1] of a supercurrent flowing at zero voltage through a superconductor-barrier-superconductor sandwich, is one of the most fascinating macroscopic quantum-mechanical effects in condensed matter physics. The original theoretical[1] and experimental[2] work concentrated on superconductor-insulator-superconductor (SIS) tunnel junctions which have a hysteretic (double-valued) current-voltage characteristic. Ambegaokar and Baratoff[3] showed that for thin tunnel junctions, the characteristic voltage (product of the critical current at zero voltage I_c and the normal state resistance R_n) is determined solely from the size of the superconducting gap Δ; i.e. it is independent of the properties of the insulator. It was soon realized that the Josephson effect also occurred when the barrier was a normal metal (N) through the proximity effect as expressed by Andreev bound states.[4] Boguliubov and de Gennes,[5] and Gor'kov[6] developed real-space formulations of the Bardeen–Cooper–Shrieffer[7] theory, that allow one to microscopically

model inhomogeneous Josephson junctions. The quasiclassical approach then progressed with the introduction of the (general) Eilenberger[8] and (dirty) Usadel[9] equations, which were simplifications appropriate for ballistic and diffusive junctions, respectively. The challenge was to determine the proper boundary conditions for the partial differential equations that were appropriate for the experimental situations to be analyzed and to include self-consistency in the calculations. On the experimental side, new efforts focusing on ScS junctions[10] (where c denotes a geometrical constriction) were shown to be particularly suited to the quasiclassical approach, as the superconductivity was not diminished in the superconductor as one approached the interface of the geometrical constriction (and both the boundary conditions and the self-consistency became trivial). IBM embarked on a significant application effort,[11] where they created digital electronic circuits out of Pb and PbO based tunnel junctions and so-called latching technology (where the switching occurs between the zero voltage and finite-voltage parts of the I–V curve). It became apparent that this latch-based technology would never be fast enough to be competitive with the limits of semiconductor technology, so the IBM project waned in the early 1980's.

This was unfortunate, because a number of new breakthroughs occurred in the 1980's including the Nb-Al-AlO_x-Nb process, developed at Bell Laboratories,[12] which is used today for state-of-the-art low-T_c based digital electronics; the Blonder–Tinkham–Klapwijk[13] model, which illustrated how multiple Andreev reflections can explain subharmonic gap structures in the I–V characteristic of SNS junctions; the development of rapid-single-flux-quantum (RSFQ) logic[14] which showed how to make digital circuits run at the fastest possible speeds that superconducting electronics are capable of (and requires nonhysteretic single-valued I–V characteristics); and the discovery of high-temperature superconductors[15] which may be able to operate at speeds much in excess of a THz. Finally, the interest in mesoscopic superconductivity[16] and nanotechnology have pushed efforts in the quasiclassical approach and Landauer-type approaches[17] to the point where it is a well-developed tool to describe low-temperature junctions in the clean and dirty limits. Some milestones of the quasiclassical approach are the prediction that I_cR_n can be increased over the Ambegaokar–Baratoff limit in point-contact junctions,[18] the ability to describe microscopic properties of SINIS junctions,[19] the application of multiple Andreev reflection theory[20] to submicron, self-shunted tunnel junctions,[21] and the understanding of how disorder modifies a clean junction through processes that take place at the Thouless energy.[22]

The success of the quasiclassical approach is dramatic and has been reviewed by numerous authors.[23] Nevertheless, there have been a number of new experimental results that examine Josephson junctions in regimes that lie outside the region of validity of the quasiclassical approach. These include (i) high-T_c-based junctions[24] where the barrier is a correlated insulator with a charge redistribution occurring at the interface with the superconductor (grain boundaries, ion-damaged, interface engineered, or Co-doped junctions); (ii) highly transparent SSmS junctions[25]

(Sm denotes a heavily doped semiconductor playing the role of a phase-coherent N) where the barrier can have its properties tuned by engineering the doping of the semiconductor (which is usually chosen to be either Si or InAs); (iii) SCmS junctions[26] (Cm denotes a correlated metal) where the barrier is a correlated metal (or insulator) that lies close to the metal–insulator transition (such as TaN_x); and (iv) mesoscopic short ballistic proximity-effect junctions[27] where the transport through the barrier is ballistic, but the barrier thickness is less than the normal metal coherence length. These are junctions that may have technological importance and which provide a number of theoretical challenges.

Our approach is complementary to the quasiclassical methods. We begin from a self-consistent many-body physics technique that automatically accounts for correlation effects and is best suited for short-coherence length superconductors (since there is no averaging over the Fermi length λ_F). It uses the dynamical mean field theory[28] approach, as modified for inhomogeneous systems by Potthoff and Nolting.[29] We review briefly how these calculations are performed, but concentrate mainly on illustrating and explaining the results as applied to SNS and SNSNS structures,[30] SCmS junctions,[31,32] SINIS junctions[33] where the insulating layers are created by a mismatch of the Fermi energies of the S and N producing the charge redistribution of a screened dipole layer, and ballistic proximity-effect junctions.[34]

The coherence lengths in technologically interesting low-T_c materials range from approximately 40 nm in Nb,[35] to 24 nm in NbTiN films,[36] to 5 nm in Nb_3Sn,[37] to a range of 1–5 nm for c-axis MgB_2.[38] In high-T_c materials, the coherence length is typically[39] about 0.3 nm along the c-axis and 1–2 nm in the ab-plane. We choose to examine relatively short coherence length s-wave superconductors here, with the coherence length ranging from about 1–2 nm depending on the size of the unit cell (a more complete description is given below).

We focus mainly on the figure-of-merit (or characteristic voltage) I_cR_n of the junction. Typical values in low-T_c junctions lie in the range between 50 μV and 1.5 meV. The characteristic voltage determines the operating speed of a Josephson junction circuit element using RSFQ logic because the integral (over time) of the voltage pulse is equal to a flux quantum; hence the width of the pulse is inversely proportional to the height of the pulse which is determined by the characteristic voltage. This figure-of-merit has been analyzed in a number of different situations: (i) Ambegaokar and Baratoff[3] showed that $I_cR_n = \pi\Delta/2e$ for tunnel junctions with vanishingly thin I layers (Δ is the superconducting gap in the bulk); (ii) Kulik and Omelyanchuk[18] showed that for clean point-contact SNS junctions one has $I_cR_n = \pi\Delta/e$ and for dirty (diffusive) point-contact junctions one has $I_cR_n = 2\pi\Delta/(3e)$; Bardeen and Johnson[40] and Ishii[41] showed that long junctions have $I_cR_n \propto ev_F/L$; and (iv) Freericks, Nikolić, and Miller[31] showed that for clean wide three-dimensional SNS junctions, the characteristic voltage is limited by the product of the bulk critical current times the Sharvin[42] resistance, which typically is close to the above values. Experimentally, one finds a wide range of characteristic

voltages, especially as the barrier material is chosen to be a N, a Cm, a Sm, or a hybrid SINIS or SNSNS structure. One of the fundamental questions is how can one maximize the characteristic voltage while maintaining nonhysteretic I–V characteristics (tunnel junctions can be made nonhysteretic by shunting them with a low resistance metal shunt, which reduces the effective characteristic voltage, and thereby reduces performance, and requires more area for the shunted junctions on the chip).

Another aspect of the problem that is important for high current density, short coherence length junctions is the issue of self consistency.[43,44] The superconducting order parameter Δ (or more correctly, the pair amplitude F which is the ratio of the order parameter to the interaction strength U; $F = \Delta/|U|$) can be suppressed in the superconductor over a length scale on the order of the bulk superconducting coherence length (called the "inverse proximity effect"). In junctions where such a situation occurs, self consistency is critical for determining how the superconductivity varies through the junction and in determining the size of the supercurrent when there is a phase gradient over the system. In addition, if the superconducting gap is large enough that the ratio of Δ to the Fermi energy μ (measured from the bottom of the band) is nonnegligible, then there is intrinsic scattering induced by so-called Δ/μ terms.[45] Our calculational methods are inherently self-consistent, as the DMFT requires self consistency to properly determine the effects of many-body correlations. This ensures current conservation within our junctions.

2. Formalism

The junctions that we model contain stacked infinite planes, consisting of superconducting and barrier materials (B). The junction is divided into two pieces — (i) a bulk superconducting piece and (ii) a self-consistently determined superconductor-barrier-superconductor piece. This is illustrated schematically in Fig. 1 where we show a self-consistent piece of 4 superconducting planes, 2 barrier planes, and 4 superconducting planes, embedded in semi-infinite bulk superconductors on the left and the right. In our calculations, we always choose 30 self-consistently determined superconducting planes, and from 1 to 80 barrier planes (the word "barrier" is used to generically describe the "weak-link" material which can be a N, Sm, Cm, or a more complicated hybrid structure). The planar directions are denoted by x and y, while the inhomogeneous direction (perpendicular to the planes) is called the z direction.

The system is discretized to a lattice (of lattice constant a) that represents the unit cells of the underlying ionic lattice of the junction. This allows one to include arbitrary bandstructure and pairing symmetry effects.[46] We choose a simple cubic lattice with a nearest neighbor hopping integral $t = 1$ to describe the conduction band (we choose the hopping integral to be the same for the S and the B for simplicity; this choice can be relaxed at the cost of introducing additional parameters). The S is modeled by an attractive Hubbard model,[47] with an instantaneous attraction

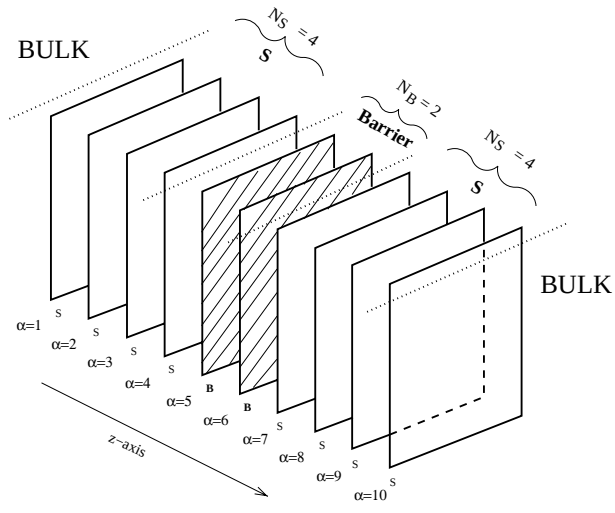

Fig. 1. Inhomogeneous planar structure of the modeled Josephson junction. The junction is separated into two pieces: (i) a bulk superconductor piece and (ii) a self-consistently determined superconductor-barrier-superconductor sandwich. In calculations reported here, we always use 30 S planes (about 8 times the bulk coherence length) and the barrier size ranges from 1 to 80 planes.

$U = -2$. The Hubbard model is solved by an s-wave Hartree–Fock approximation, which is equivalent to the BCS approximation[7] except that the energy cutoff is determined by the electronic bandwidth rather than the phonon frequency.[44] The bulk superconducting transition temperature is $T_c = 0.112$ and the superconducting gap at zero temperature is $\Delta = 0.198$, which yields the expected BCS gap ratio $2\Delta/k_B T_c \approx 3.6$. The bulk coherence length ξ_S is found by fitting the decay of the pair amplitude F due to the "inverse proximity effect" at the SN interface.[30] We find $\xi_S \approx 3.7a$, which agrees well with the BCS prediction of $\xi_S = \hbar v_F^S/\pi\Delta$ with v_F^S chosen as an appropriate average over the Fermi surface (for lattices with a lattice constant $a \approx 0.3$–0.6 nm, we find $\xi_S \approx 1$–2 nm). The bulk critical current per unit area is $I_{c,bulk} = 0.0289(2et)/\hbar a^2$. The value of our bulk critical current density is slightly higher than the one determined by a Landau depairing velocity $v_d = \Delta/\hbar k_F$ ($j_{c,bulk} = env_d$, where the density of electrons is $n = k_F^3/2\pi^2$, assuming a spherical Fermi surface) because of the possibility to have gapless superconductivity in three dimensions at superfluid velocities slightly exceeding[48] v_d (note that k_F is direction-dependent for a cubic lattice at half-filling). Calculations on our junction are performed at a temperature of $T = 0.01$, which is effectively at the zero-temperature limit ($T/T_c \approx 0.09$) for the superconducting properties.

The barrier material will be chosen to be either a clean normal metal (which has $U = 0$) or an annealed binary disordered material described by the spin-one-half Falicov–Kimball model.[49] The Falicov–Kimball model has two types of particles: (i) conduction electrons (which do not interact with themselves) and (ii) static ions,

which can be thought of as classical particles that occupy a lattice site i if $w_i = 1$ and do not occupy a lattice site if $w_i = 0$. There is an interaction between the conduction electrons and the static ions denoted by U_i^{FK}, which results in an annealed binary distribution of the disorder. When the barrier is a clean normal metal, then one can calculate the coherence length of the junction to be $\xi_0 = \hbar v_{\mathrm{F}}^{\mathrm{N}}/(\pi\Delta)$; in junctions where the hopping integral and Fermi level in the S and N are chosen to be the same, we always have $\xi_0 = \xi_{\mathrm{S}}$. This result does not hold in Sm barriers, because there is usually significant mismatch of the Fermi velocities, yielding different length scales. Nor does it hold in Cm junctions where the concept of a Fermi velocity is ill defined, and the length scale ξ_0 can only be estimated by mapping onto an effective disordered Fermi liquid and comparing the diffusive Thouless energy to the superconducting gap.

The final interaction that we have in our system is a long-range classical Coulomb interaction, which generates a self-consistently determined electric potential V_i^{C}. This Coulomb interaction arises when the chemical potential of the S differs from that of the B. When these materials are assembled to form a Josephson junction, the overall chemical potential is fixed to be that of the S. The B layers then are at the wrong chemical potential, so a charge redistribution occurs, with charge shifting most near the SB interface. The value of the Coulomb potential V^{C} at the αth plane is found by adding the potentials from every other plane that has a total electronic charge that differs from the bulk charge density of the respective plane (S or B). These potentials cause a local shift of the chemical potential equal to $V_i = eV_i^{\mathrm{C}}$. These potentials must be self-consistently calculated, so that the potential shift at a given plane, is equal to precisely the magnitude of shift needed to create the redistributed charge density of the plane (a more complete discussion will be given below). If the chemical potentials of the bulk S and B are equal to each other, then all V_i vanish.

Hence the Hamiltonian of the junction is

$$H = -\sum_{\langle ij\rangle\sigma} c_{i\sigma}^{\dagger} c_{j\sigma} + \sum_i U_i \left(c_{i\uparrow}^{\dagger} c_{i\uparrow} - \frac{1}{2}\right)\left(c_{i\downarrow}^{\dagger} c_{i\downarrow} - \frac{1}{2}\right) + \sum_{i\sigma} U_i^{\mathrm{FK}} c_{i\sigma}^{\dagger} c_{i\sigma}\left(w_i - \frac{1}{2}\right) + \sum_i (V_i + \Delta E_{\mathrm{F}})\left(c_{i\uparrow}^{\dagger} c_{i\uparrow} + c_{i\downarrow}^{\dagger} c_{i\downarrow}\right), \qquad (1)$$

where $c_{i\sigma}^{\dagger}$ ($c_{i\sigma}$) creates (destroys) an electron of spin σ at site i on a simple cubic lattice, $U_i = -2$ is the attractive Hubbard interaction for sites within the superconducting planes, U_i^{FK} is the Falicov–Kimball interaction for planes within the barrier, w_i is a classical variable that equals 1 if a disorder ion occupies site i and is zero if no disorder ion occupies site i, V_i is the self-consistently determined Coulomb potential energy (if there is a charge redistribution), and $\Delta E_{\mathrm{F}} = E_{\mathrm{F}}^{\mathrm{N}} - E_{\mathrm{F}}^{\mathrm{S}}$ is the mismatch of Fermi levels in the S and B (ΔE_{F} always vanishes in the S, but may be nonzero in the B). A chemical potential μ is employed to determine the filling. The superconductor is always chosen to be at half filling here ($n_{\mathrm{S}} = 1$), hence $\mu = 0$.

We employ a Nambu–Gor'kov formalism[6,50] to determine the many-body Green's functions. Details of the algorithm appear elsewhere.[30,31,33] Since the junction is inhomogeneous in the z-direction only, we have translational symmetry in the planar directions. We begin by converting the three-dimensional problem into a quasi-one-dimensional problem, by using the method of Potthoff and Nolting.[29] We perform a Fourier transformation within each plane to determine the mixed-basis Green's function [defined in terms of two-dimensional momenta (k_x and k_y) and the z-coordinate of the plane] under the assumption that the electronic self energy is local, but can vary from plane to plane (in other words, the self energy has no k_x of k_y dependence, but does depend on z). For each momentum in the two-dimensional Brillouin zone, we have a one-dimensional problem with a sparse matrix, since the only coupling between planes is due to the hopping to each neighboring plane. The infinite "block-tridiagonal" matrix can be inverted by employing the renormalized perturbation expansion,[51] which calculates both the single plane and the nearest neighbor Green's functions. A final summation over the two-dimensional momenta produces the local Green's function and the Green's function for propagation from one plane to its neighboring plane. The DMFT is then employed to calculate the local self energy from the local Green's function and then the local Green's function is calculated from inverting the quasi-one-dimensional matrix. For the S or N, this amounts to just the Hartree–Fock approximation; for the Falicov–Kimball model, the exact solution corresponds to the coherent potential approximation (within the Nambu–Gor'kov formalism). These steps are repeated until the Green's functions have converged to a fixed point, where we have a self-consistent solution of the inhomogeneous problem that allows for nonuniform variations in both the pair-field correlations and in the phase. One important consistency check is total current conservation at each plane in the self-consistent region. There can be discontinuities in the current at the bulk-superconductor–self-consistent superconductor interface; the superconducting gap has always healed at this point, but there can be a jump in the phase (since this is far from the Josephson junction, it has a negligible effect on the results). This computational algorithm is a generalization of the conventional Boguliubov–de Gennes approach to allow for correlations within the barrier.

This algorithm can be carried out for the normal state or for the superconducting state on the imaginary or real frequency axes. We work on the real axis in order to calculate the normal state resistance and the interacting DOS. Since we have a many-body system, we must use Kubo's formula for the conductivity. Details for this calculation appeared elsewhere.[30,33] Our formalism calculates the conductivity by neglecting vertex corrections and evaluating the simple bubble diagram (which is exact in the infinite-dimensional limit[52]).

3. Results for SNS Junctions

We begin by examining Josephson junctions where the barrier material is a normal metal, corresponding to $U = 0$, $\langle w \rangle = 1/2$, and $U_{\mathrm{FK}} = 0.05$. We choose the

Falicov–Kimball interaction to be nonzero, because it makes the numerical computations converge more rapidly (by introducing damping), yet the transport through the normal metal remains ballistic, with a mean-free-path much longer than the barrier thickness.

The first thing we will investigate is the critical current per unit cell. We can determine the dc Josephson current within an imaginary-axis calculation. We begin by calculating the supercurrent in the bulk superconductor when a uniform phase gradient is applied to the anomalous Green's functions (or equivalently the anomalous self energy). The bulk supercurrent increases monotonically with the phase gradient until the bulk critical current density is reached. Then we use this bulk solution for the boundary conditions of the superconductor and employ the computational algorithm described above to calculate the local self energy (and Coulomb potentials, if relevant) on each plane. Next, we calculate the Green's functions (on the imaginary axis) that create an electron on the $(\alpha + 1\text{st})$ plane and destroy an electron on the αth plane. The current passing through the αth plane is a simple integral of this Green's function.[30] A strict convergence criterion is local current conservation — that the current through each of the self-consistent planes agrees to one part in 10^3. Once the current is determined for a given bulk phase gradient, it is important to determine the total phase difference over the barrier, in order to calculate the current-phase relation. Since the barrier is spatially extended, and because the bulk superconductor has a uniform phase gradient over it, the total phase over the barrier must be carefully defined. We choose the following procedure: (i) first, we define the barrier region (of $N_{\rm B}$ planes) to correspond to the region that lies in between the midpoint of each SB interface ($z_{\rm L} = N_{\rm S} + 1/2$, $z_{\rm R} = N_{\rm S} + N_{\rm B} + 1/2$); (ii) the phase difference over the barrier (of thickness $L = N_{\rm B}a$) is determined by the total phase change over the barrier region, which corresponds to the uniform phase gradient $L\nabla\phi$ plus a phase deviation term $\delta\phi(z_{\rm R}) - \delta\phi(z_{\rm L})$; and (iii) since the phase is defined only at each lattice point, we define the phase deviation at $z_{\rm L}$ and $z_{\rm R}$ as the average of the phase deviation at the two neighboring lattice points {i.e., $\delta\phi(z_{\rm L}) = [\delta\phi(N_{\rm S}) + \delta\phi(N_{\rm S}+1)]/2$ and similarly for the right hand side}. In most calculations, we can only determine the increasing part of the current-phase relation, where the current increases monotonically from 0 to $I_{\rm c}$, but in some cases, we find that in the self-consistent region we can determine some of the "unstable branch" of the current-phase relation, where the current decreases as the total phase difference increases. In these cases, there must be a jump in the superconducting phase at the bulk S-self-consistent S boundaries (since the bulk supercurrent is always increasing with increasing bulk phase gradient). This does not affect our results much though, because the bulk S-self-consistent S boundary lies far from the barrier of the Josephson junction, and the current is uniform within the self-consistent region.

We plot the current-phase relation for a variety of SNS barrier thicknesses (1, 2, 4, 6, 8, 10, 14, 20, 30, 40, and 60) in Fig. 2 (more correctly, we plot the current per unit cell area a^2). The dotted line is the bulk critical current density. One can see immediately that for thin junctions, where the $I_{\rm c}$ approaches that of the bulk

superconductor, the junction can never build too much total phase over it, so the current-phase relation is far from sinusoidal. As the total critical current of the junction decreases (as the thickness L increases), we find that the current-phase relation becomes more and more sinusoidal. This is illustrated further in the inset, where we plot the renormalized current-phase relation $I(\phi)/I_c$. The deviation from sinusoidal behavior for high current junctions, with the critical phase difference being much less than $\pi/2$, arises entirely from the self-consistency.[43] But it can be understood in a simple fashion, since the superconductivity is not too strongly reduced for a thin normal metal barrier, the majority of the phase difference is the bulk phase gradient multiplied by the thickness of the barrier. As the thickness gets small, the total phase across the junction must also be small, hence we get the behavior shown in Fig. 2. Note that the maximum of $I(\phi)$ always occurs below $\pi/2$. This difference from the analytical predictions[40,41] of π for thick SNS junctions happens because of the self consistency.[43]

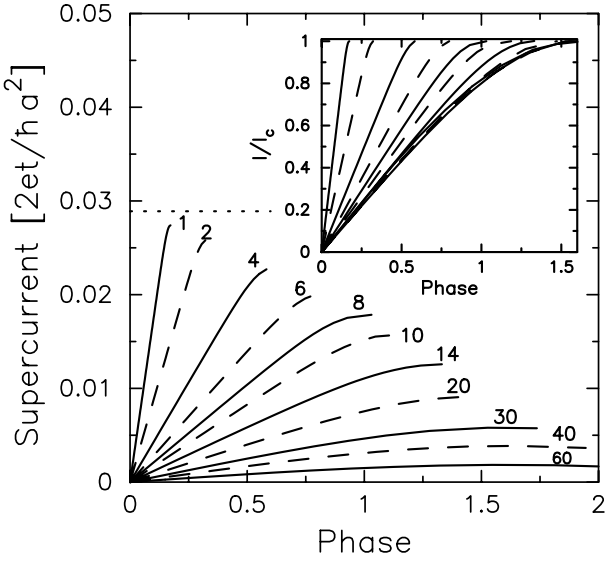

Fig. 2. Current-phase relations for SNS junctions ranging from thin ($N_B = 1$) to thick ($N_B = 60$) barriers. The dotted line is the value of the critical current (for a unit square) in the bulk superconductor. Inset is the renormalized current-phase relation $I(\phi)/I_c$ to show how thick the junction needs to be before sinusoidal behavior is restored ($N_B = 20$ is thick enough for sinusoidal behavior). The deviation is due to self-consistency.

It is interesting to examine how the phase deviation behaves as the bulk phase gradient is increased from zero to the gradient corresponding to the critical current. Here we show such a plot for an intermediate thickness $N_B = 20$ in Fig. 3. These results are generic for most junctions. The phase deviation starts off negative, goes through zero at the center of the barrier, and then becomes positive (in a mirror image) of the negative function. What this tells us is that the majority of the phase

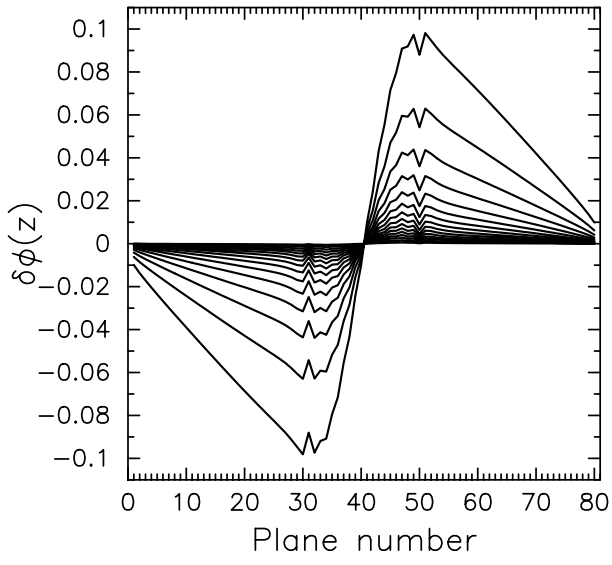

Fig. 3. Phase deviation as a function of the plane number for a SNS junction with $N_B = 20$. The barrier begins at plane 31. Each curve corresponds to a different bulk phase gradient in the S leads, which increases from zero up to the critical current. Note how the largest phase gradient occurs at the center of the barrier. The total phase gradient (bulk plus deviation) is always positive.

change, or in other words the maximal phase gradient, occurs at the center of the barrier. This is where the superconductivity is the smallest. The critical current is determined by the maximal phase gradient that the central plane of the barrier can support and still maintain current conservation. Note further, the "notch" in the curves at the SN boundaries.[34] This jump first smooths out, and then disappears as correlations are introduced. The phase-deviation curves are well-behaved and smooth for correlated SCmS junctions. In the case of thinner SNS junctions, the phase deviation curves develop an unusual "phase antidipole structure" for small current (where the slope of the phase deviation is *negative* at the center of the barrier), that disappears as the critical current is approached.[34] The phase antidipole is the opposite of the phase dipole behavior discovered in narrow SNS junctions.[53] We don't plot that behavior here.

This behavior can be understood better if we directly examine the proximity effect for the Josephson junction. As described above, the pair-field amplitude F is a better measure of the superconductivity than the gap function Δ because the gap is always zero within the normal metal. The proximity effect is plotted in Fig. 4 for a variety of junction thicknesses. The first thing to notice about the proximity effect is the suppression of F within the S as one approaches the SN boundary. The shape of this suppression is independent of the thickness of the junction, once the thickness is larger than a few bulk S coherence lengths. The exponential healing of F to its bulk value within the S occurs over the length scale of ξ_S. Fitting the decay to an exponential gives a coherence length of $\xi_S = 3.7a$. Such a suppression of the

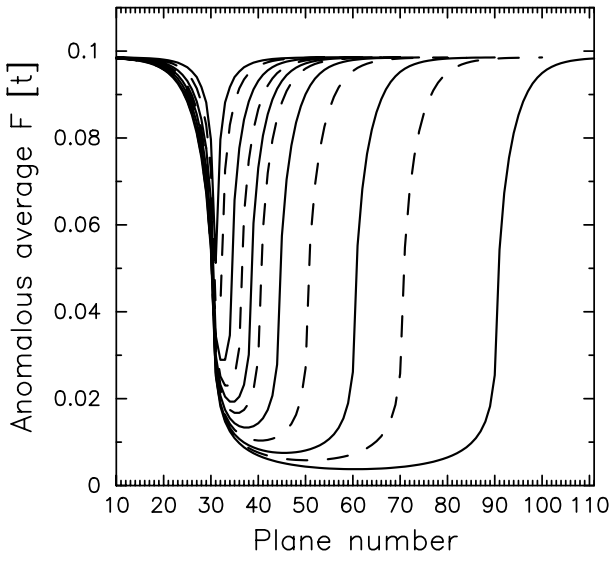

Fig. 4. Anomalous pair field F versus plane number for a variety of junction thicknesses (1, 2, 4, 6, 8, 10, 14, 20, 30, 40, and 60) and vanishing supercurrent. Note how the shape of F at the SN boundary does not depend on thickness once the junction is thicker than twice the bulk coherence length $N_{\mathrm{B}} > 8$, and how the magnitude of F at the central plane is determined by the thickness of the junction and the N coherence length ξ_{N}.

superconductivity can be mimicked in the quasiclassical approach by introducing the so-called suppression parameter γ_{S}, but such calculations are rarely performed self-consistently. Here the decay and healing of the superconductivity is determined from the parameters of the microscopic Hamiltonian. It is important to note that for thin junctions $L < 2\xi_{\mathrm{S}}$, the value of F at the SN interface (plane 30) and the critical current of the junction depend strongly on the thickness of the junction.[34] Once L becomes large enough, the value of F near the SN interface is "frozen in" and the critical current is determined by the Thouless energy (for L on the order of ξ_0) or by the normal metal coherence length ξ_{N} (for L larger than ξ_{N}).

The next thing to notice is that the magnitude of F on the central plane of the barrier is determined solely from the (ballistic) N coherence length $\xi_{\mathrm{N}} = \hbar v_{\mathrm{F}}/2\pi k_{\mathrm{B}}T \approx 35 - 40a$ (once the barrier is thick enough). As the barrier is made thicker and thicker, one can see how the pair-field decays exponentially with the thickness. For thinner junctions it is hard to detangle the two length scales, but for thicker junctions, one can clearly see the difference between ξ_0 and ξ_{N} in Fig. 4.

Finally, we can understand much about the current-phase relations, and the phase-deviation plot when we combine it with the proximity-effect plot of F. Note that as the magnitude of F decreases toward the center of the barrier, we find that the phase gradient is maximal at this central plane, since the magnitude of F is the smallest there. This is the only way that one can maintain current conservation from plane to plane. Hence, the critical current of the junction is found by the

maximal phase gradient that can be sustained at the central plane of the barrier. This explains, in a simple way, why the ($T > 0$) critical current decays exponentially (over the length scale $\xi_{\rm N}$) as the thickness increases, since the magnitude of F decreases exponentially (for L large enough), and the maximal phase gradient is always the same order of magnitude.

One final observation is in order. In the majority of the cases that we perform calculations for, there is little change in the proximity effect [i.e. in $|F(z)|$] as one increases from zero supercurrent flow up to $I_{\rm c}$. In thick junctions, we see very little variation. As the junctions are made thinner, there are changes which are typically on the order of a few percent (but sometimes becoming large for very thin junctions).

In addition to examining imaginary axis (equilibrium) thermodynamic properties, we can also examine (equilibrium) dynamic properties. The most interesting quantity to calculate is the interacting density of states (DOS) at each plane in the self-consistent region. For a ballistic N junction, we know that the density of states should show the presence of Andreev bound state peaks (which will be broadened by the coupling to the infinite leads and the sum over the transverse two-dimensional momentum), and we expect to see the density of states linearly approach zero at zero frequency within the barrier due to the presence of quasiparticles with vanishingly small longitudinal momentum.[54] In Fig. 5(a) we plot the DOS at the central plane of a moderately thick $L = 10a$ SNS junction for zero supercurrent, moderate supercurrent ($I = I_{\rm c}/4$), and larger supercurrent ($I = I_{\rm c}/2$). As the current increases, we see that the peaks corresponding to the Andreev bound states move apart, due to the expected Doppler shift, since the Andreev bound states come in time-reversed pairs — one carries current to the right and one to the left. As supercurrent is passed through the junction, time-reversal symmetry is broken and the degeneracy of these states is lifted, because one state moves in the direction of the supercurrent flow, and one moves in the opposite direction. This can be clearly seen in the splitting of the peaks as supercurrent flows, which increases with increasing current. As the current is increased further, we find our computational algorithm breaks down on the real axis due to phase slips. In panel (b), we show the evolution of the minigap (in an $L = 5a$ SNS junction) as the attractive Coulomb interaction is reduced in magnitude. As expected for Δ/μ scattering effects, we see that the minigap decreases in magnitude as the coupling strength decreases. In panel (c), we plot the local DOS as a function of plane number (with current $I_{\rm c}/8$ flowing through the junction) ranging from the center of the barrier (plane 34), to the SN interface (plane 30), to a length approximately $\xi_{\rm S}$ inside the S (plane 25), to deep within the S (plane 10). Note how within the barrier, there is little dependence of the DOS on position (except for a small reduction near the minigap), and how the ABS leak far into the S (much farther than $\xi_{\rm S}$) and have relatively large spectral weight close to the SN boundary. Such effects can only be seen in self-consistent calculations. Finally in panel (d), we plot the current carrying DOS at the same small supercurrent as in (c) ($I = I_{\rm c}/8$). The supercurrent is found by an integral

of the current carrying DOS weighted by the appropriate Fermi factors. Note how the peaks of the current DOS correspond closely to the shifting Andreev peaks, confirming that the split peaks carry current in opposite directions.

Surprisingly, the DOS does not decrease linearly to zero[54] [see panels (a) and (b)], but rather shows the appearance of a minigap at the lowest energies. This behavior is different from what is expected from the quasiclassical situations, and we believe it arises from the fact that the superconductor has so short a coherence length that one cannot neglect Δ/μ effects[45] (which are beyond quasiclassic methods) as illustrated most clearly in panel (b). As the junction is made thicker, the minigap decreases, and the linearly vanishing behavior is restored by the time $L = 20a$. The results for the DOS then agree with all of our expectations from the quasiclassical theory (once L is thick enough). This shows that our many-body formalism is able to properly capture the regime described by the quasiclassical theory. But, as we will see below, it can go beyond this to account for correlation effects as well. Another point to emphasize is that the minigap depends only weakly on the amount of current flowing through the junction. This is also contrary with the minigap that arises in quasiclassical situations, which show a decreasing minigap with supercurrent. This "theoretical spectroscopy" of a Josephson junction would be interesting to observe experimentally, and preliminary studies with tens of nm wide probes have already been performed.[55] It would be interesting to examine some of these junctions with the finer spatial resolution of an STM tip.

The other dynamical property that yields much information about the junction is the normal state resistance R_{n}. We calculate the normal state resistance by ignoring the superconductivity (setting $F = 0$), and using the Kubo formula for the conductivity. In performing our calculations, we neglect the effect of vertex corrections, which is exact in the large dimensional limit.[52]

In a ballistic SNS junction, like the ones that we study here, the normal state resistance is essentially independent of the thickness L of the junction, and is given by the Sharvin[42] resistance. Since the critical current depends exponentially on L for thick junctions (with characteristic length ξ_{N}), we expect the $I_{\mathrm{c}}R_{\mathrm{n}}$ product to decrease once the thickness becomes larger than the N coherence length. Recent experiments[27] showed anomalous behavior for SSmS junctions created out of Nb and heavily doped InAs. In particular, the characteristic voltage was seen to be much smaller than the Kulik–Omelyanchuk limit for a clean SNS junction. This should not come as a surprise, because there is a large Fermi velocity mismatch in these junctions, so the interfaces must have significant scattering even in "highly transparent" junctions. Whenever such scattering is present, one expects a reduction from the Kulik–Omelyanchik limit. Here we examine the best possible scenario for the Kulik–Omelyanchuk limit, where there is no extrinsic scattering at the interface, and the only reductions to the $I_{\mathrm{c}}R_{\mathrm{n}}$ product can arise from the proximity and "inverse" proximity effects or finite Δ/μ scattering.

In our junctions, we have no geometric constriction for the barrier, so the maximal characteristic voltage, in the clean limit, is just the product of the

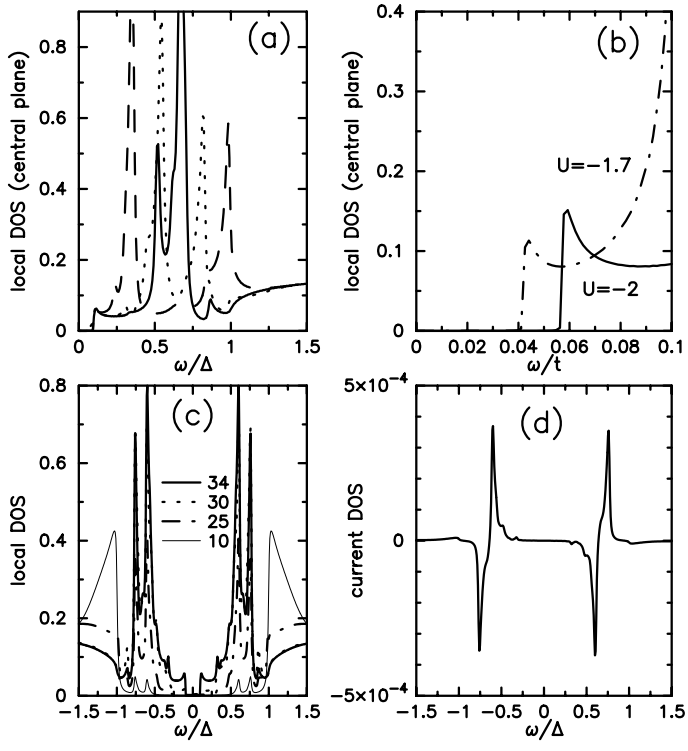

Fig. 5. Many-body density of states as a function of frequency for $L = 10a$. (a) The solid line is with no supercurrent, the dotted line with moderate supercurrent $I_c/4$, and the dashed line for larger supercurrent $I_c/2$, at the central barrier plane. Note how the DOS has a minigap at small frequency, and how the peaks, corresponding to Andreev bound states, move apart as supercurrent flows through the junction. (b) Detail of the minigap for $U = -2$ (solid line) and $U = -1.7$ (chain-dotted line) and $L = 5a$. Note how the reduction of the size of the minigap for weaker interactions indicates that the likely source of the minigap is the so-called Δ/μ scattering. (c) Local DOS as a function of plane number for $I = I_c/8$. Note how the ABS leak far into the superconductor (distances much larger than ξ_S), a result that could not be seen with non-self-consistent calculations. (d) Current-carrying density of states at the central barrier plane for $I = I_c/8$.

bulk critical current with the Sharvin resistance of the infinite S leads. For our three-dimensional system, the product of these two is about one-half the Kulik–Omelyanchuk limit and equals $1.45\Delta/e$. What we find, is that even for junctions that have $L < \xi_N \approx 35-40a$, the characteristic voltage is sharply reduced (e.g. $I_c R_n$ is an order of magnitude smaller than the thin-junction limit when $L \approx 40a$), similar to what is seen in experiment, but the effect isn't quite strong enough to produce the behavior seen in experiment (where the reduction in $I_c R_n$ was estimated to be about two orders of magnitude). The reason for the decrease in our calculations is a combination of the "inverse proximity effect" and the proximity effect, which reduce the superconductivity and thereby limit the amount of supercurrent that can flow through the junction. Such effects can only be found in self-consistent calculations.

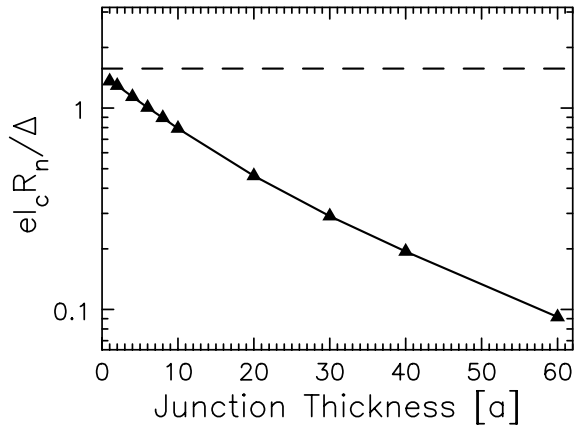

Fig. 6. Semilogarithmic plot of the characteristic voltage versus junction thickness L for ballistic SNS junctions. The dashed line is the clean planar junction limit. Note how the characteristic voltage is suppressed dramatically below the clean planar limit due to the "inverse proximity effect" and the proximity effect.

We will see in the next section how a charge redistribution at the SN interface (due to Fermi-level mismatch) reduces the characteristic voltage even further and is one possible way to explain the experimental behavior.

Our work on SNS junctions has produced a number of interesting behaviors for short-coherence-length Josephson junctions. We found that the critical current is determined by the maximal phase gradient that can be sustained over its "weakest link" — the central plane of the barrier. We also saw that because of the "inverse proximity effect" (where the superconductivity is reduced in the S as one approaches the SN interface) and the proximity effect (where superconductivity is reduced as one enters the N), the critical current has a strong dependence on the thickness of the junction. Since the normal-state resistance is essentially independent of the thickness, this provides a partial explanation for why the characteristic voltage of ballistic SNS junctions may be much smaller than predicted by analytic means. The reason is that the self-consistency, as seen through the proximity effects, sharply reduces the critical current, and thereby reduces the characteristic voltage. We verified, in a striking fashion, how the Andreev bound states split due to the presence of a supercurrent flowing through the junction, arising from the Doppler shift. Finally, we saw the appearance of a minigap for thin junctions, which gave way to the expected linear vanishing of the DOS as the junction is made thicker.

4. SINIS Junctions from Double-Barrier Screened-Dipole Layers

When two different metals are placed together in a hybrid structure, there is usually a mismatch of the Fermi levels. This means that one of the metals will have a chemical potential that differs from its equilibrium value. As a result charge will be redistributed at the interfaces between the metals until an overall equilibrium

situation returns, where the charge deviates from the bulk values in the metals over a length scale (called the Debye screening length $l_{\rm D}$) near the interfaces. This process should occur in SNS Josephson junctions as well. If the redistribution of charge is large enough, then it can create a SINIS junction, where the I layers are formed by the screened-dipole layers that appear at each SN interface.

Hybrid SINIS junctions have been studied over the past two decades.[19,33,56] The basic idea is that one can combine the attractive properties of both SIS and SNS junctions by constructing hybrid SINIS junctions. The most heavily studied SINIS junctions are made out of the conventional Nb-Al-AlO$_x$ process, with additional layers grown to create the more complicated structures. In some cases Nb is used in the barrier, which is a situation we will discuss in more detail in the next section. While much effort has been expended on trying to optimize junction properties, no one has been able to create reproducible SINIS junctions with high enough critical currents and characteristic voltages to be competitive with submicron, self-shunted tunnel junctions. These Nb-Al-AlO$_x$-based junctions are described well by the quasiclassical approach,[19] and we do not concern ourselves with them here.

Instead, we concentrate on SINIS junctions where the I layers are self-consistently generated by screened-dipole layers in materials (such as the high-$T_{\rm c}$ grain-boundary junctions[57] or doped[58] InAs junctions) where the Debye screening length is a few lattice spacings (rather than less than an Angstrom, which is seen in most conventional metals). In this regime, quasiclassical techniques are not applicable, because the redistributed charge profile requires one to take into account the modifications of the Green's functions on length scales on the order of the Fermi length[59] $\lambda_{\rm F}$. Quasiclassical techniques can only be attempted in materials where the screening length is so small that the potential from the screened-dipole layer can be represented by a delta function. These spatially extended boundaries, however, are perfectly suited for our many-body approach.

We use a combined quantum-classical technique to determine the self-consistent solution of the SINIS junctions. Quantum mechanics is used to determine the equilibrium charge density in each plane, subject to the given chemical potential and the current value of the local potential shift V_i. Next, we determine the charge deviation $\delta n(z) = n(z) - n_{\rm Bulk}$, where $n_{\rm Bulk} = n_{\rm N}$ or $n_{\rm S}$ if the plane is a normal metal or a superconductor, respectively. Once the charge deviations are known at each plane, we use classical electrostatics to determine the total potential shift at each plane, by summing the potential shifts (due to the constant electric fields emanating from each plane with a charge deviation) from every other plane. This then determines the total Coulomb potential at site i, $V_i^{\rm C}$, and the potential energy shift $V_i = eV_i^{\rm C}$ at each plane. Once the new potential energy shift is known, then we use the quantum-mechanical algorithm to calculate the charge densities at each plane, and repeat the process until the potentials and charge densities have converged to a fixed point.

This procedure is time-consuming, and adds greatly to the computational effort needed to find a self-consistent solution. Fortunately, in most cases, the charge

profile does not change much with either the supercurrent flowing through the system, or the temperature, so once the charge profile has been determined for one calculation, it serves as a good guess for the charge profile of the next calculation with similar parameters. Use of this "numerical annealing" strategy greatly reduces the number of computational cycles needed to achieve convergence of numerical results.

In Fig. 7, we plot the charge profile for Josephson junctions with $L = 20a$, a variety of Fermi-level mismatches $\Delta E_{\mathrm{F}} = E_{\mathrm{F}}^{\mathrm{N}} - E_{\mathrm{F}}^{\mathrm{S}}$, and $l_{\mathrm{D}} \approx 3a$. The bulk superconductor filling is chosen always to be half filled $n_{\mathrm{S}} = 1$. In (a)–(b) the normal metal filling is also half-filled $n_{\mathrm{N}} = 1$, while in (c)–(d) it is much smaller $n_{\mathrm{N}} = 0.01$, to mimic the behavior in a doped semiconductor. Note how the charge deviation (and the corresponding potential barrier) grows as the Fermi-level mismatch increases in (a). We need only consider positive Fermi-level mismatch in this case, because particle-hole symmetry gives the same result for negative mismatches. One might note that the general shape of the charge profile looks the same for different mismatches. This is confirmed in (b), where we rescale the charge profile, by dividing by ΔE_{F}. The curves all collapse onto each other. We believe this occurs because the noninteracting density of states is quite flat near half filling for a simple cubic lattice. Indeed, when we look at the data in panel (d), which does not have any symmetry between positive and negative values, nor has the shape independent of the size of the Fermi level mismatch, we see that scaling does not hold for this data (which we believe is because the density of states is quite asymmetric and has strong energy dependence near the Fermi level of the "doped semiconductor").

Recent Raman scattering experiments[58] on Nb-InAs bilayers show a dramatic change in the Raman response as a function of the temperature as one cools through the superconducting transition of the Nb. One interpretation of these results, is that the effective Debye screening length, or equivalently, the charge profile at the interface, changes dramatically as one goes through T_{c}. We see no evidence of this in our calculations, but we always fix the Debye screening length (or more precisely the optical dielectric constant ϵ_∞) in our calculations, and we see changes of the charge distribution no larger than a few percent as one cools through T_{c} (the only exception is when ΔE_{F} is on the order of T_{c} or Δ, where sizable changes in the potentials, but not the screening lengths, are seen). It is our belief that if the spatial extent of the charge accumulation region is changing as one goes through T_{c}, then it must require a proper treatment of the nonlocal screening effects, which is beyond our computational techniques.

The next thing we examine is the proximity effect, shown in Fig. 8. In (a) we show the case with $n_{\mathrm{N}} = 1$ ($\Delta E_{\mathrm{F}} = 1$, 2, 3, 5, and 10) and in (b) we show $n_{\mathrm{N}} = 0.01$ ($\Delta E_{\mathrm{F}} = 1$, -1, -3, and -10). As the charge deviation increases, and the potential barrier increases, we see that the "inverse proximity effect" decreases as expected, and approaches the behavior expected for rigid boundary conditions (step function in Δ at the interface). But as the barrier increases further, due to larger mismatches, the "inverse proximity effect" gets larger and larger. This

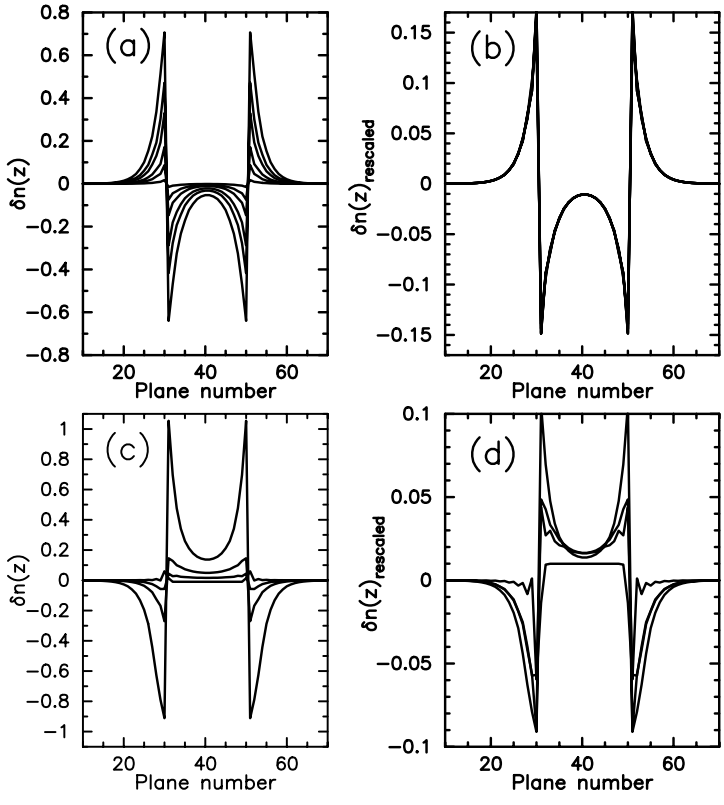

Fig. 7. Charge redistribution in a SINIS Josephson junction with (a-b) $n_{\rm N} = 1$ and (c-d) $n_{\rm N} = 0.01$. The charge deviation $\delta n(z)$ is plotted for a number of different values of the Fermi level mismatch $\Delta E_{\rm F}$ ($\Delta E_{\rm F} = 0.1$, 0.5, 1, 2, 3, and 5 for $n_{\rm N} = 1$ and $\Delta E_{\rm F} = 1$, -1, -3, -10 for $n_{\rm N} = 0.01$). The values of $\Delta E_{\rm F}$ decrease from the bottom line to top (at plane 35) in panels (a, c, and d). Panels (b) and (d) show rescaled plots, where we divide the charge deviation by $\Delta E_{\rm F}$. Note how the charge redistribution scales for the half-filled (metallic) case, but does not for the semiconductor case. The distributions are symmetric for positive and negative $\Delta E_{\rm F}$ in (a-b), but not in (c-d).

effect is due entirely to the modification of the local charge on the planes near the interface, and the fact that the Debye screening length is chosen to be a few lattice spacings. Note how the presence of a scattering charge barrier at the interface sharply reduces the superconductivity within the N. This is a consequence of the reduced transparency due to the charge-redistribution-induced scattering. In the case of the "doped semiconductor", we find that for small mismatches $|\Delta E_{\rm F}| < 1$, the proximity effect does reproduce the expected rigid boundary conditions, with the added feature of small oscillations (due to Fermi-length effects) near the interface. But as the mismatch is made more negative, one reproduces the same kind of enhanced "inverse proximity effect", as was seen at half filling, due to the charge redistribution within the superconductor. Note that the step-function boundary conditions for small mismatch are most likely due to the fact that there is

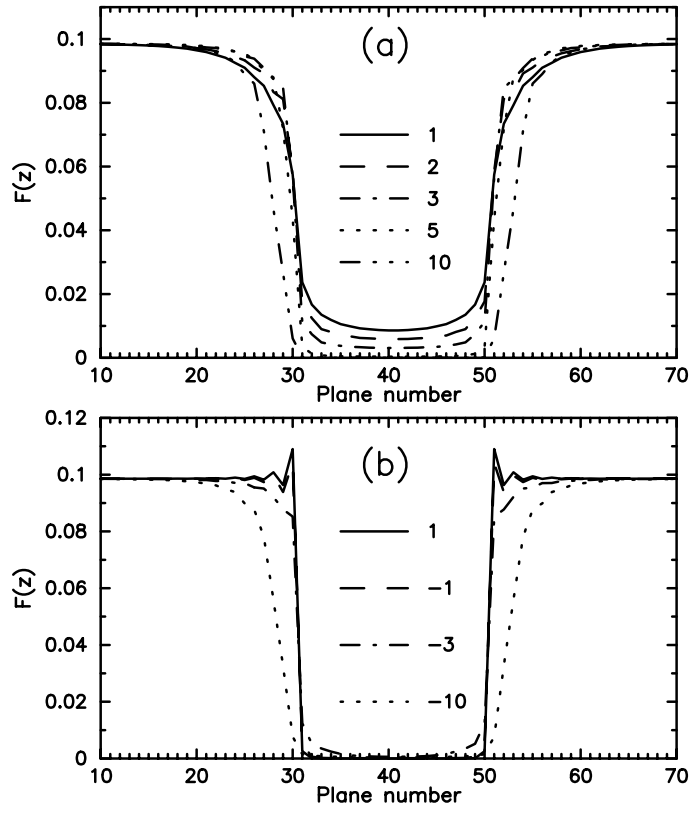

Fig. 8. Proximity effect for (a) $n_{\mathrm{N}} = 1$ and (b) $n_{\mathrm{N}} = 0.01$. Note how, in (a), the "inverse proximity effect" first is reduced as the barrier height increases, but then the "inverse proximity effect" gets larger, as the spatially extended barrier increases in magnitude. In (b), we recover rigid boundary conditions for small mismatch (plus Fermi-length oscillations), which then disappear as the barrier gets larger. Note also how the proximity effect is sharply reduced as the barrier gets larger.

a huge Fermi-wavevector mismatch in this junction, which causes large scattering, and reduces the transparency of the junction to the point where the conditions for rigid boundary conditions hold. The appearance of the small oscillations would not be seen in a quasiclassical approach, that averages over short length scales.

Our final result is the characteristic voltage versus the junction thickness for three different Fermi level mismatches in Fig. 9. The critical current decreases monotonically with the thickness, in nearly all cases. The normal state resistance, can be enhanced dramatically for intermediate sized junctions, where the thickness is less than twice the Debye screening length. Once the thickness is greater than $2l_{\mathrm{D}}$, the resistance is virtually independent of the thickness, as expected for ballistic junctions. It is mainly this anomalous behavior at intermediate thicknesses, which leads to the nonmonotonic behavior of the characteristic voltage. When we compare $I_{\mathrm{c}}R_{\mathrm{n}}$ to the SNS case, we see that for thicker junctions, the characteristic

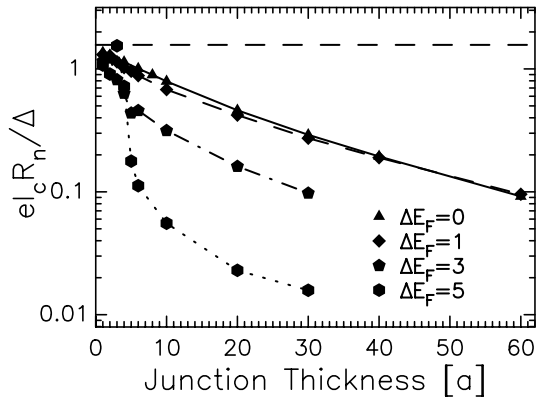

Fig. 9. Semilogarithmic plot of the characteristic voltage versus junction thickness L for ballistic SINIS junctions. The dashed line is the clean planar junction limit. Note how the characteristic voltage is suppressed dramatically below the clean planar limit for thicker junctions, but can be enhanced when the junction thickness is on the order of the Debye screening length ($\Delta E_{\rm F} = 5$ and $N_{\rm B} = 3$). Note that a small barrier $\Delta E_{\rm F} = 1$ does not change much from the case with no Fermi-level mismatch.

voltage is sharply reduced when there is additional scattering due to a screened-dipole layer. This arises mainly from the fact that the critical current is reduced more rapidly with thickness for thicker junctions. But, surprisingly, there is an intermediate regime, of relatively thin junctions (similar to grain-boundary junctions in high-$T_{\rm c}$), where the characteristic voltage can be enhanced by the charge redistribution ($\Delta E_{\rm F} = 5$ and $N_{\rm B} = 3$).

We find that when a screened dipole layer develops at a SN interface due to Fermi-level mismatch, it usually produces a sharp reduction in the characteristic voltage, because the critical current is reduced much more than the normal-state resistance (because of the large reduction of the proximity effect due to the scattering from the extended charge barrier). This is clearly not advantageous for digital electronics applications (or for power applications in multigrain high-$T_{\rm c}$ tapes). It appears that junction qualities should be improved if the Fermi-level mismatch can be reduced by an educated choice of materials used in the junctions.

5. SNSNS Junctions with Enhanced $I_{\rm c}R_{\rm n}$ Products

We saw in the previous section that if we allow charge to redistribute due to a Fermi level mismatch, then it usually has a deleterious effect on the characteristic voltage. If we recall that the critical current (of a SNS junction) is determined by the maximal phase gradient that the weakest plane can sustain, and that the normal state resistance is dominated by the Sharvin resistance in clean systems, then one way to enhance the characteristic voltage is to improve the superconductivity within the central planes of the barrier, while maintaining quantum coherence throughout

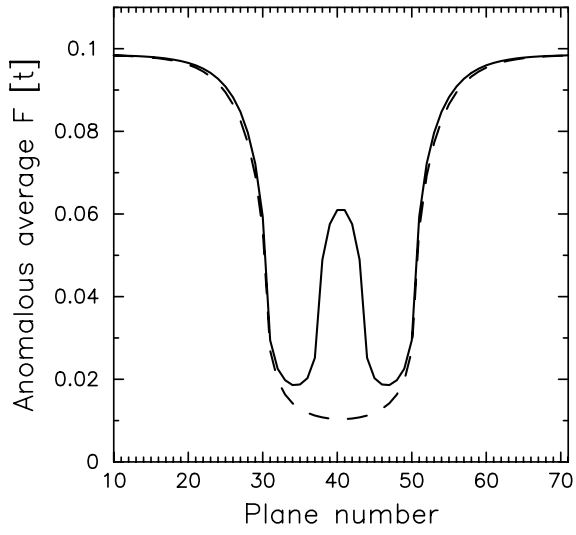

Fig. 10. Proximity effect for a SNSNS junction (solid line), where the central 6 planes of a SNS junction (with $N_B = 20$) are replaced by S planes compared to the proximity effect in the SNS junction (dashed line). Note how the proximity effect is sharply enhanced within the central S part of the junction due to the enhanced superconductivity in that region. This enhancement leads to a significantly enhanced I_c (in fact, the ratio of the enhanced $I_c R_n$ value of about 1.7 is close to the ratio of the minimal value of F in the two junctions, which is about 1.8).

the whole junction. This motivates the consideration of SNSNS junctions, where one replaces the central planes of the N barrier with S. Recent experiments[56] have indicated that one can get a dramatic rise in the characteristic voltage, which has been confirmed theoretically.[30]

Here we will explore a simple system, where we take the 20 barrier planes and replace the middle 6 planes with S. In Fig. 10, we plot the proximity effect within this junction, and see that the proximity effect is enhanced due to the extra superconducting planes (the minimal F is about twice as large in the SNSNS junction than in the SNS junction). Because of this, the critical current is sharply enhanced, increasing by a factor of two over that of a similar SNS junction with $L = 20a$. Since there are additional interfaces, which will add to the scattering, the resistance will be increased too, but since it is dominated by the Sharvin contribution, it remains essentially the same. The net effect is a near doubling of the characteristic voltage to $0.775\Delta/e$ ($I_c R_n = 0.461\Delta/e$ for the $L = 20a$ SNS junction); it still remains much lower than the maximal analytic limit of $\pi\Delta/e$.

Even more interesting is a plot of the many-body DOS as a function of position within the SNSNS plane (see Fig. 11). The leftmost SN boundary is at plane 30, the inner NS boundary is at plane 37, the inner SN boundary at plane 44, and the rightmost NS boundary is at plane 50. One can see interesting structure in the Andreev bound states. The main peak at approximately $\pm 0.6\Delta$ remains at about the same energy in the interior S planes and in the N. As we move into the N, away

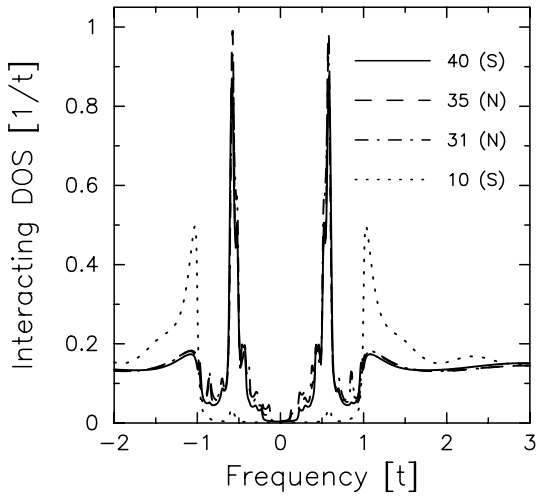

Fig. 11. Many-body density of states as a function of position in the SNSNS junction. The solid curve is at plane 40, at the center of the innermost S layers; the dashed curve is at plane 35 just inside the N metal; the chain-dotted curve is at plane 31, at the SN boundary, and the dotted line is at plane 10, approximately $5\xi_S$ away from the SN boundary within the bulk S. Note how the main Andreev peak at 0.6Δ remains essentially unchanged within the interior of the junction (and even has some weight deep within the S). We see an additional development of spectral weight near both the minigap and near the bulk gap in the N relative to the innermost S layers. The appearance of the minigap for this junction arises from the increased Δ/μ scattering due to the additional two SN (NS) interfaces.

from the innermost S planes, there is a small spectral weight shift to lower energies, near the minigap in the DOS, and at about 0.9Δ where a small peak develops in the N. Note that even though the $L = 20a$ SNS junction has no minigap, we find a sizable minigap here, because it is determined by the Δ/μ scattering at each of the (now four) SN interfaces. As we move deep into the superconductor (approximately $5\xi_S$ from the bulk SN interface at plane 10), we still see a remnant of the Andreev bound state peak in the superconductor at about 0.6Δ, and a recovery of the expected BCS density of states elsewhere. Similar problems have also been investigated by Lodder and coworkers.[60]

We see that there are complicated structures that can lead to dramatic enhancements of the characteristic voltage. In particular, replacing some of the central planes of the N barrier by S will enhance the proximity effect and thereby enhance I_c, and will also typically enhance the normal state resistance due to extra interfaces. This result has been seen already in experiment.[56] What is interesting, is that if the S layers are thin enough, then the general character of the ABS remain unchanged within the hybrid junction, and the net effect is an increase in the characteristic voltage of the junction. What may prove to be more problematic in these junctions is whether or not they are stable to changes in temperature, which is necessary for implementation within digital electronics.

6. SCmS Junctions Tuned Through a Metal–Insulator Transition

The final type of junction we will consider here is quite different from the others, and has not been analyzed with quasiclassical approaches, because it lies well outside the region of validity for quasiclassics. It is a SCmS junction, where the correlated metal is described by the Falicov–Kimball model, tuned to lie close to the metal–insulator transition in the bulk. Depending on precisely where one sits in the phase diagram, one can tune the metal–insulator transition to occur either at a fixed thickness, by increasing the interaction strength, or at a fixed interaction strength, by increasing the thickness L of the barrier.[31]

The Falicov–Kimball model is always a non-Fermi liquid, because the presence of static disorder always creates a finite lifetime to putative quasiparticles at the Fermi surface.[31] Initially, this behaves like a "disordered" Fermi liquid, but as the interaction increases in strength, there is a transition in the many-body DOS to a pseudogap structure, where there is a dip at the Fermi level, followed shortly thereafter by a true gap developing at the chemical potential for $U_{\mathrm{FK}} > 4.9$. If $U_{\mathrm{FK}} > 4.9$, then a metal–insulator transition occurs as a function of the thickness of the barrier (since a single plane barrier $[N_{\mathrm{B}} = 1]$ is never insulating for transport perpendicular to the plane). Similarly, if we fix the barrier thickness, then there is a metal–insulator transition as a function of U_{FK}.

In Fig. 12, we first examine the proximity effect for the case where $N_{\mathrm{B}} = 5$, which is just slightly larger than the bulk coherence length of the S. When U_{FK} is small, the junction behaves similarly to a SNS junction, with both "inverse" and conventional proximity effects. As U_{FK} increases to larger than 6, we first see the "inverse proximity effect" reduced, with the development of small oscillations due to "Fermi-surface effects", but the most striking development is of sharp oscillations, with a large amplitude within the barrier that are tied to the SB interfaces. We believe that these oscillations arise from properties of an insulating barrier being brought in contact with a superconductor. Oscillations develop at each SB interface over a length scale on the order of ξ_0, which can interfere if the barrier is thin enough. We find that as the barrier is made thicker, the oscillations quickly die off as a function of distance from the SB interface (but the amplitude near the interface remains large).

As disorder scattering is added to the barrier of a junction, a new energy scale, called the Thouless energy[61] E_{Th} starts to play a role in determining properties of the junction. The Thouless energy is defined to be $E_{\mathrm{Th}} = \hbar\mathcal{D}/L^2$, with $\mathcal{D}$ the classical diffusion constant. One of the most important predictions of the quasiclassical approach, is that the interacting DOS develops a minigap on the order of E_{Th} near the chemical potential for a "disordered" Fermi liquid in a confined mesoscopic geometry.[62] This gap increases in size as the disorder increases until it reaches a maximum at some fraction of the superconducting gap, and then the dirty limit takes over. This modification of the DOS in the normal metal, from essentially constant, to possessing a low-energy "minigap" is one of the most interesting

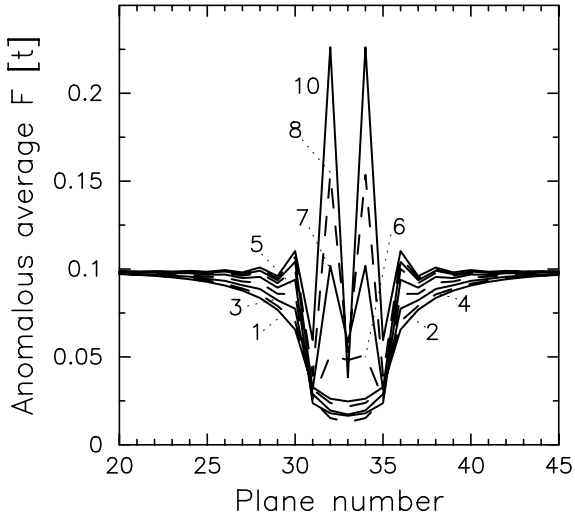

Fig. 12. Proximity effect for a SCmS junction with $L = 5a$. Note how the shape of the anomalous average smoothly changes from that of a SNS junction, with a large "inverse proximity effect", to that of a SI interface, with a relatively flat F in the superconductor (plus small oscillations). The interesting result is the large amplitude oscillation occurring within the barrier, which dies off in a length scale on the order of ξ_0. The curves alternate from solid and dashed lines for $U_{\rm FK} = 1$, 2, 3, 4, 5, 6, 7, 8, 10.

consequences of the proximity effect, when analyzed in a quasiclassical approach (especially its evolution with increasing disorder[63]).

The behavior in a Cm is quite different. We plot in Fig. 13 the many-body DOS at the central plane of a $L = 10a$ SCmS junction (i.e., for the plane at the center of the barrier), for values of $U_{\rm FK}$ ranging from 0.1 to 2. When $U_{\rm FK} = 0$, a minigap appears in the DOS as seen in Fig. 5. As scattering is introduced, the minigap shrinks, eventually disappearing and becoming a pseudogap as $U_{\rm FK}$ increases. For small $U_{\rm FK}$ we see the characteristic development of a minigap at low energy, but we see another energy scale enters as well at about five times the minigap, where a "soft" pseudogap appears. As $U_{\rm FK}$ increases further, this picture evolves, with the gaps remaining intact, but narrowing, until a critical value of $U_{\rm FK} \approx 0.8$ is reached, and the minigap disappears. The DOS continues to fill in at low energies, with the remnants of a pseudogap remaining until $U_{\rm FK}$ becomes large enough that the DOS loses all low-energy structure. Note further, that as the scattering increases, by increasing $U_{\rm FK}$, we find that the Andreev bound states, occurring just below the superconducting gap, first broaden dramatically, then get washed out of any structure as the correlations increase further. *In fact, it is likely that the destruction of the minigap is occurring because of the extensive broadening of the Andreev bound states.*

What is interesting, is that all of the behavior of the closing of the minigap occurs well before the pseudogap develops in the bulk many-body DOS of the

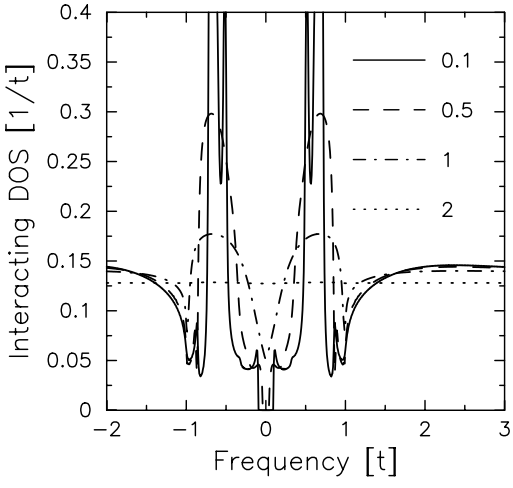

Fig. 13. Many-body density of states at the central plane of a $L = 10a$ SCmS junction. The correlation strength U_{FK} is increased from 0.1 to 2. Note how we first see a minigap that disappears as the correlations increase and becomes a pseudogap, before vanishing entirely into a structureless, flat "background".

Falicov–Kimball model. Another surprise is that if we extract the diffusion constant from the normal-state resistance, we find that the size of the gap is much smaller than the quasiclassical prediction[64] of $3.12E_{\mathrm{Th}}$. In addition, we found that the size of the gap does not scale inversely as L^2, as it must in the quasiclassical theory. Hence the proximity effect in a correlated metal has very different characteristics than what is seen in a disordered Fermi liquid.

We now turn to the question of optimizing the characteristic voltage of a SCmS junction. In Fig. 14, we show plots of the characteristic voltage versus U_{FK} for four different thicknesses of the barrier $L = a$, $2a$, $5a$, and $20a$. The dashed line is the Ambegaokar–Baratoff prediction.[3] A thin junction ($L = a$) behaves pretty much as expected. $I_{\mathrm{c}}R_{\mathrm{n}}$ lies below the planar junction limit for small U_{FK} and increases modestly as the scattering increases, reaching an optimization near $U_{\mathrm{FK}} = 2$. As one goes through the metal–insulator transition, the characteristic voltage saturates, and becomes independent of U_{FK}. It lies about 15% below the Ambegaokar–Baratoff prediction though, because of the "inverse proximity effect" and the averaging over an anisotropic "Fermi surface". When we double the number of planes to two, we find similar behavior at small U_{FK} with a mild optimization of $I_{\mathrm{c}}R_{\mathrm{n}}$ near $U_{\mathrm{FK}} = 3$, but the characteristic voltage continues to increase without any apparent bound as U_{FK} increases in the insulating regime. This is quite different from the Ambegaokar–Baratoff prediction. Of course, we expect the junctions to be hysteretic when the system is a good insulator. The behavior for the intermediate-sized junction $L = 5a$ is the most interesting. In the metallic region, the characteristic voltage decreases monotonically with U_{FK} until we hit the metal–insulator transition. At that point $I_{\mathrm{c}}R_{\mathrm{n}}$ increases by more than a factor of 2, shows a mild optimization near $U_{\mathrm{FK}} = 7$,

and then decreases for larger U_{FK}. This illustrates the proposition that $I_{\mathrm{c}}R_{\mathrm{n}}$ can be optimized near the metal–insulator transition, and be higher than the Ambegaokar–Baratoff prediction. We examine the final case of a thick junction $L = 20a$ in panel (d). Here, the characteristic voltage decreases sharply with U_{FK}, with the rate being fastest near the metal–insulator transition. We believe the very low values on the insulating side occur because the normal state resistance, being thermally activated, has strong temperature dependence even at these low temperatures, which leads to the extremely low values of the characteristic voltage.

Finally, we produce a "Thouless plot" of our data, by fixing U_{FK} and studying the characteristic voltage as a function of the barrier thickness. We consider three cases: (i) $U_{\mathrm{FK}} = 2$, a strongly disordered metal; (ii) $U_{\mathrm{FK}} = 4$, a pseudogap metal; and (iii) $U_{\mathrm{FK}} = 6$, a correlated insulator with a small gap. A quasiclassical prediction,[22] shows that the characteristic voltage smoothly changes from the Kulik–Omelyanchuk limit[18] to being proportional to E_{Th} for thick junctions. The crossover is a universal curve in the ratio of the Thouless energy to the superconducting gap. We plot this behavior in Fig. 15. The Thouless energy is determined by first fitting the exponential decay of the supercurrent with L to extract the barrier coherence length ξ_{B}. The Thouless energy is then $E_{\mathrm{Th}} = 2\pi k_{\mathrm{B}}T\xi_{\mathrm{B}}^2/L^2$.

Note that both metallic curves ($U_{\mathrm{FK}} = 2$ and 4) fall on essentially the same curve, illustrating the "universality" of the quasiclassical prediction.[22] This may be a little surprising, because the pseudogap metal is clearly outside of the realm of the quasiclassical approach. The correlated insulator has a nonuniversal shape, that deviates sharply from that of the metals. The characteristic voltage is initially quite flat for thin junctions, and then is reduced sharply with thickness for thicker junctions. Because of this behavior, we expect the Josephson coupling to be very sensitive to thickness when L is larger than the crossover between the metal and the insulator (where the curve decreases sharply). In this region, the Josephson coupling can be much larger for slightly thinner barrier regions, and much smaller for slightly thicker regions. This behavior can look like pinholes, but will occur, even if the barrier is homogeneous, and has a small variation in its thickness (perhaps even as small as one monolayer). We believe this kind of behavior may occur in high-T_{c} junctions, which have much larger spreads in their junction parameters even in well controlled fabrications runs.

We found a number of new behaviors in correlated-barrier Josephson junctions. In particular, there is an anomalous enhancement of the proximity effect at the SB interface, as the barrier is made more insulating. In addition, we found a wide variety of different characteristic voltages, with an optimization on the insulating side of the metal–insulator transition for intermediate-thickness junctions. We also saw remarkable behavior in the interacting DOS, where the quasiclassical prediction of a minigap, disappears as correlations increase, and broaden the ABS in the DOS; first the minigap is replaced by a pseudogap, and then it becomes a structureless flat background as the correlations increase further; this effect is most likely due to "lifetime" effects that broaden the Andreev bound states into wide, featureless

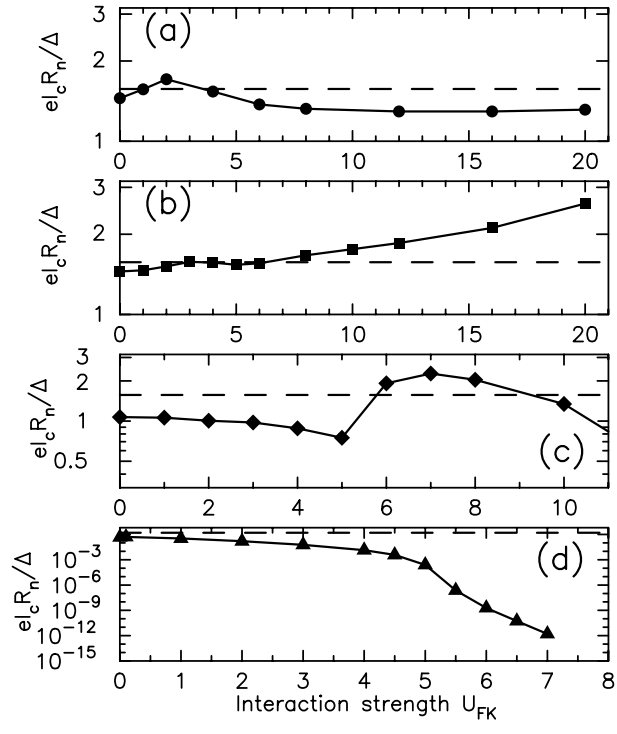

Fig. 14. Semilogarithmic plot of the characteristic voltage versus $U_{\rm FK}$ for four different junction thicknesses: (a) $L = a$; (b) $L = 2a$; (c) $L = 5a$; and (d) $L = 20a$. The dashed line is the Ambegaokar–Baratoff prediction of $I_cR_n = 1.57\Delta/e$. Note how in (a) we do reproduce the Ambegaokar–Baratoff prediction of the characteristic voltage being independent of $U_{\rm FK}$ in the insulating regime, but the value is somewhat smaller in magnitude. In (b), we see that I_cR_n appears to increase without limit. In (c), we find an optimization, above the Ambegaokar–Baratoff prediction, just on the insulating side of the metal–insulator transition. And in (d), we find I_cR_n decreases dramatically with $U_{\rm FK}$.

resonances. Finally, we found that correlated insulating barriers can have an intrinsic pinhole effect, when the thickness lies close to the critical thickness of the metal–insulator transition.

7. Conclusions

We have illustrated many of the novel results that can be analyzed with a new approach toward modeling Josephson junctions, that are relevant for short-coherence-length junctions with either correlated barriers, or barriers with potentials that have features on atomic length scales. In this review, we have emphasized the physical properties, since the formalism has been developed elsewhere.[30,31,33] We examined many different types of junctions, ranging from SNS, to SNSNS, to SINIS, to SISmIS, to SCmS. We found a number of interesting results that are not seen in the quasiclassical theory. These include (i) a sharp reduction in the characteristic volt-

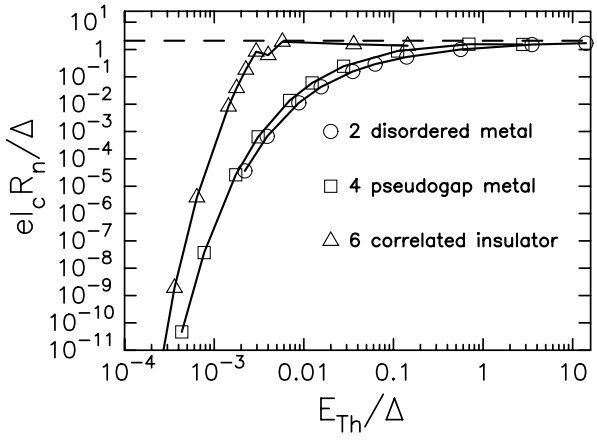

Fig. 15. Thouless plot for $U_{\mathrm{FK}} = 2$, 4, and 6. The characteristic voltage is plotted against the Thouless energy. Note that both metallic cases ($U_{\mathrm{FK}} = 2$ and 4) do fall on a nearly "universal" curve, which is similar in shape to that seen in quasiclassics.[22] The insulating curve, however, deviates from this form, having a flat curve for thin junctions, and then a sharp decrease after the thickness-tuned metal–insulator transition. This behavior leads to the possibility of what we call an intrinsic pinhole effect.

age when a mismatch of Fermi levels causes a screened-dipole layer; (ii) a large enhancement of $I_{\mathrm{c}}R_{\mathrm{n}}$ for SNSNS junctions; (iii) the disappearance of the minigap due to increased scattering in correlated barriers; (iv) an optimization of $I_{\mathrm{c}}R_{\mathrm{n}}$ for a correlated insulator close to the metal–insulator transition; and (v) the prediction of an "intrinsic pinhole" effect for correlated insulating barriers due to deviations from universality in the Thouless plot. These results can explain a number of anomalous results seen in experiments on Josephson junctions ranging from ballistic SSmS junctions to high-T_{c}-based junctions.

The use of dynamical mean field theory in modeling properties of inhomogeneous structures like Josephson junctions allows us to calculate properties of a number of systems that lie outside of the successful quasiclassical approach which include short-range potentials, correlated systems, and structures with thicknesses on the order of the Fermi length. These techniques can easily be used for other types of devices, such as hybrid superconducting and ferromagnetic structures, with potential applications to spintronics and quantum computing. In future work, we will generalize these results to allow nonequilibrium properties (such as the I–V characteristic) to be calculated, to allow unconventional pairing symmetry (like d-wave) for the superconductors for a better simulation of high-T_{c} devices, and to allow ferromagnetic states for simulating spintronic devices.

Acknowledgments

We are grateful to the Office of Naval Research for funding under grant number N00014-99-1-0328. Real-axis analytic continuation calculations were partially

supported by the National Computational Science Alliance under grant number DMR990007N (utilizing the NCSA SGI/CRAY ORIGIN 2000) and were partially supported by a grant of HPC time from the Arctic Region Supercomputer Center. We wish to acknowledge useful discussions with A. Brinkman, T. Van Duzer, L. Greene, J. Ketterson, T. Klapwijk, K. Likharev, J. Luine, J. Mannhart, I. Nevirkovets, N. Newman, I. Roshchin, J. Rowell, S. Tolpygo, and D. Van Vechten.

References

1. B. D. Josephson, *Phys. Lett.* **1**, 251 (1962).
2. P. W. Anderson and J. M. Rowell, *Phys. Rev. Lett.* **10**, 230 (1963).
3. V. Ambegaokar and A. Baratoff, *Phys. Rev. Lett.* **10**, 486 (1963).
4. A. F. Andreev, *Zh. Eksp. Teor. Fiz.* **46**, 1823 (1964) [*Sov. Phys. JETP* **18**, 1228 (1964)]; I. O. Kulik, *Zh. Eksp. Teor. Fiz.* **57**, 1745 (1969) [*Sov. Phys. JETP* **30**, 944 (1970)].
5. N. N. Bogoliubov, V. V. Tolmachev and D. V. Shirkov, *A New Method in the Theory of Superconductivity* (Consultants Bureau, New York, 1959); P. G. de Gennes, *Superconductivity of Metals and Alloys* (Addison-Wesley, New York, 1966).
6. L. P. Gor'kov, *Zh. Eksp. Teor. Fiz.* **34**, 735 (1958) [*Sov. Phys. JETP* **7**, 505 (1958)].
7. J. Bardeen, L. Cooper and J. Schrieffer, *Phys. Rev.* **108**, 1175 (1957).
8. G. Eilenberger, *Z. Phys.* **B214**, 195 (1968).
9. K. D. Usadel, *Phys. Rev. Lett.* **25**, 507 (1970).
10. K. K. Likharev, *Rev. Mod. Phys.* **51**, 101 (1979).
11. See for example *IBM J. Res. Develop.* **24**, 105–264 (1980).
12. M. Gurvitch, M. A. Washington and H. A. Huggins, *Appl. Phys. Lett.* **42**, 472 (1983).
13. G. E. Blonder, M. Tinkham and T. M. Klapwijk, *Phys. Rev.* **B25**, 4515 (1982); T. M. Klapwijk, G. E. Blonder and M. Tinkham, *Physica* **109–110B**, 1657 (1982).
14. O. A. Mukhanov, V. K. Semenov and K. K. Likharev, *IEEE Trans. Magn.* **MAG-23**, 759 (1987); K. K. Likharev, in *Applications of Superconductivity* ed. H. Weinstock (Kluwer, Dordrecht, 2000), Ch. 5.
15. J. G. Bednorz and K. A. Müller, *Z. Phys.* **B64**, 189 (1986).
16. See special issue of *Superlattices and Microstruct.* **25** No. 5/6 (1999).
17. C. W. J. Beenakker, *Rev. Mod. Phys.* **69**, 731 (1997); C. J. Lambert and R. Raimondi, *J. Phys.: Condens. Matter* **10**, 901 (1998).
18. I. O. Kulik and A. N. Omelyanchuk, *Fiz. Nizk. Temp.* **3**, 945 (1977) [*Sov. J. Low. Temp. Phys.* **3**, 459 (1977)].
19. M. Yu. Kupriyanov and V. Lukichev, *Sov. J. Low Temp. Phys.* **8**, 526 (1982); M. Yu. Kupriyanov, A. Brinkman, A. A. Golubov, M. Siegel and H. Rogalla, *Physica C* **326-327**, 16 (1999); A. Brinkman and A. A. Golubov, *Phys. Rev.* **B61**, 11297 (2000).
20. D. Averin and A. Bardas, *Phys. Rev. Lett.* **75**, 1831 (1995); A. Bardas and D. Averin, *Phys. Rev.* **B56**, R8518 (1997).
21. Y. Naveh, V. Patel, D. V. Averin, K. K. Likharev and J. E. Lukens, *Phys. Rev. Lett.* **85**, 5404 (2000).
22. P. Dubos, H. Courtois, F. K. Wilhelm, A. D. Zaikin and G. Schön, *Phys. Rev.* **B63**, 064502 (2001).
23. W. Belzig, F. K. Wilhelm, C. Bruder, G. Schön and A. D. Zaikin, *Superlattices and Microstruct.* **25**, 1251 (1999). The limitations of the quasiclassical theories, as well as approaches which go beyond quasiclassics but within a quasiparticle picture, are reviewed in A. Altland, B. D. Simons and D. Taras-Semchuk, *Adv. Phys.* **49**, 321 (2000).

24. K. A. Delin and A. W. Kleinsasser, *Supercond. Sci. Technol.* **9**, 227 (1996); R. S. Decca, H. D. Drew, E. Osquiguil, B. Maiorov and J. Guimpel, *Phys. Rev. Lett.* **85**, 3708 (2000).
25. C. L. Huang and T. Van Duzer, *Appl. Phys. Lett.* **25**, 753 (1974); *IEEE Trans. Magn.* **MAG-11**, 766 (1975); *IEEE Trans. Elec. Devices* **ED-23**, 579 (1976); *IEEE Trans. Magn.* **MAG-13**, 862 (1977); A. Kastalsky, A. W. Kleinsasser, L. H. Greene, R. Bhat, F. P. Milliken and J. P. Harbison, *Phys. Rev. Lett.* **67**, 3026 (1991); A. W. Kleinssaser and A. Kastalsky, *Phys. Rev.* **B47**, 8361 (1993).
26. A. S. Barrera and M. R. Beasley, *IEEE Trans. Magnetics* **MAG-23**, 866 (1987); A. B. Kaul, S. R. Whitely, T. Van Duzer, L. Yu, N. Newman and J. M. Rowell, *Appl. Phys. Lett.* **78**, 99 (2001).
27. H. Takayanugi, T. Akazaki and J. Nitta, *Phys. Rev. Lett.* **75**, 3533 (1995); J. P. Heida, B. J. Van Wees, T. M. Klapwijk and G. Borghs, *Phys. Rev.* **B60**, 13135 (1999); G. Bastian, *Phys. Rev.* **B62**, 9840 (2000).
28. W. Metzner and D. Vollhardt, *Phys. Rev. Lett.* **62**, 324 (1989).
29. M. Potthoff and W. Nolting, *Phys. Rev.* **B59**, 2549 (1999).
30. P. Miller and J. K. Freericks, *J. Phys.: Condens. Matter* **13**, 3187 (2001).
31. J. K. Freericks, B. K. Nikolić and P. Miller, *Phys. Rev.* **B64**, 054511 (2001).
32. B. K. Nikolić, J. K. Freericks and P. Miller *Phys. Rev. Lett.* **88** (2002) (cond-mat/0106612).
33. B. K. Nikolić, J. K. Freericks and P. Miller *Phys. Rev.* **B65** (2002) (cond-mat/0106175).
34. B. K. Nikolić, J. K. Freericks and P. Miller *Phys. Rev.* **B64**, 212507 (2001).
35. B. W. Maxfield and W. L. McLean, *Phys. Rev.* **139**, A1515 (1965); T. Van Duzer and C. W. Turner, *Principles of Superconductive Devices and Circuits* (Elsevier, New York, 1981).
36. L. Yu, N. Newman and J. M. Rowell, *submitted to Appl. Phys. Lett.*
37. T. P. Orlando, E. J. McNiff, Jr., S. Foner and M. R. Beasley, *Phys. Rev.* **B19**, 4545 (1979).
38. C. Buzea and T. Yamashita, *Sup. Sci. Tech.* **14**, R115 (2001).
39. T. K. Worthington, W. J . Gallagher and T. R. Dinger, *Phys. Rev. Lett.* **59**, 1160 (1987); A. Kapitulnik, M. R. Beasley, C. Castellani and C. Di Castro, *Phys. Rev.* **B37**, 537 (1988).
40. J. Bardeen and J. L. Johnson, *Phys. Rev.* **B5**, 72 (1972).
41. C. Ishii, *Progr. Theor. Phys.* **44**, 1525 (1970).
42. Yu. V. Sharvin, *Zh. Eksp. Teor. Phys.* **48**, 984 (1965) [*Sov. Phys. JETP* **21**, 655 (1965)].
43. F. Sols and J. Ferrer, *Phys. Rev.* **B49**, 15913 (1994).
44. A. Levy Yeyati, A. Martín-Rodero and F. J. García-Vidal, *Phys. Rev.* **B51**, 3743 (1995); J. C. Cuevas, A. Martín-Rodero and A. Levy-Yeyati, *Phys. Rev.* **B54**, 7366 (1996).
45. M. Hurd and G. Wendin, *Phys. Rev.* **B49**, 15258 (1994).
46. A. M. Martin and J. F. Annett, *Phys. Rev.* **B57**, 8709 (1998).
47. J. C. Hubbard, *Proc. Royal Soc. London, Ser.* **A276**, 238 (1963).
48. J. Bardeen, *Rev. Mod. Phys.* **34**, 667 (1962).
49. L. M. Falicov and J. C. Kimball, *Phys. Rev. Lett.* **22**, 997 (1969).
50. Y. Nambu, *Phys. Rev.* **117**, 648 (1960).
51. E. N. Economou, *Green's Functions in Quantum Physics* (Springer-Verlag, Berlin, 1983), Appendix B.
52. A. Khurana, *Phys. Rev. Lett.* **64**, 1990 (1990).

53. R. A. Riedel, L.-F. Chang and P. F. Bagwell, *Phys. Rev.* **B54**, 16082 (1996); R. A. Riedel, M. Samanta and P. F. Bagwell, *Superlattices Microstruct.* **23**, 925 (1998).
54. D. Saint-James, *J. Phys. (France)* **25**, 899 (1964); W. L. McMillan, *Phys. Rev.* **175**, 537 (1968).
55. S. Guéron, H. Pothier, N. O. Birge, D. Esteve and M. H. Devoret, *Phys. Rev. Lett.* **77**, 3025 (1996); M. A. Sillanpaa, T. T. Heikkila, R. K. Lindell and P. J. Hakonen, cond-mat/0102367.
56. I. P. Nevirkovets and S. E. Shafranjuk, *Phys. Rev.* **B59**, 1311 (1999); I. P. Nevirkovets, J. B. Ketterson and S. Lomatch *Appl. Phys. Lett.* **74**, 1624 (1999); I. P. Nevirkovets, J. B. Ketterson, S. E. Shafranjuk and S. Lomatch, *Phys. Lett.* **A269**, 238 (2000); and unpublished.
57. A. Gurevich and E. A. Pashitskii, *Phys. Rev.* **B57**, 13878 (1998); A. Scheml, B. Goetz, R. R. Schulz, C. W. Schneider, H. Bielefeldt, H. Hilgenkamp and J. Mannhart, *Europhys. Lett.* **47**, 110 (1999); G. Hammerl, A. Schmehl, R. R. Schulz, B. Goetz, H. Bielefeldt, C. W. Schneider, H. Hilgenkamp and J. Mannhart, *Nature* **407**, 162 (2000).
58. L. H. Greene, J. F. Dorsten, I. V. Roshchin, A. C. Abeyta, T. A. Tanzer, G. Kuchler, W. L. Feldman and P. W. Bohn, *Czech. Journ. of Phys.* **46**, 3115 (1996); I. V. Roshchin, A. C. Abeyta, L. H. Greene, T. A. Tanzer, J. F. Dorsten, P. W. Bohn, S. W. Han, P. F. Miceli and J. F. Klem, unpublished.
59. A. V. Zaitsev, *Zh. Eksp. Teor. Fiz.* **86**, 1742 (1985) [*Sov. Phys. JETP* **59**, 1015 (1985)].
60. R. E. S. Otadoy and A. Lodder, cond-mat/0103277.
61. D. J. Thouless, *Phys. Rep.* **C13**, 93 (1974).
62. A. A. Golubov and M. Yu. Kupriyanov, *Sov. Phys. JETP* **69**, 805 (1989); W. Belzig, C. Bruder and G. Schön, *Phys. Rev.* **B54**, 9443 (1996); A. A. Golubov, F. K. Wilhelm and A. D. Zaikin, *Phys. Rev.* **B55**, 1123 (1996).
63. S. Pilgram, W. Belzig and C. Bruder, *Phys. Rev.* **B62**, 12462 (2000).
64. F. Zhou, P. Charlat, B. Spivak and B. Pannetier, *J. Low. Temp. Phys.* **110**, 841 (1998).